Double-crossover phenomena in Laplacian growth: Effects of sticking probability and finite viscosity ratio

Takashi Nagatani
College of Engineering, Shizuoka University, Hamamatsu 432, Japan

H. Eugene Stanley
Center for Polymer Studies, Boston University, Massachusetts 02215
(Received 6 November 1989)

A combined effect of sticking probability and finite viscosity ratio is studied on the pattern formation in Laplacian growth. A renormalization-group theory is developed to study the crossover phenomena between the diffusion-limited aggregation (DLA) and nonfractal structure. A two-stage crossover phenomenon is analyzed by using a three-parameter position-space renormalization-group method. A global flow diagram in three-parameter space is obtained. It is found that there are three nontrivial fixed points, the first Eden point, the DLA point and the second Eden point. The second Eden point corresponding to the dense structure is stable in all directions, while the first Eden point and the DLA point are saddle points. When the sticking probability P is small and the viscosity ratio is finite, the aggregate must cross over from the dense structure, through the DLA fractal, finally to the dense aggregate.

I. INTRODUCTION

Fractal growth phenomena in pattern formation[1-11] have recently attracted considerable attention. Examples of pattern formation in diffusive systems include viscous fingering, electrochemical deposition, crystal growth, and dielectric breakdown. The diffusion-limited aggregation[1,2] (DLA) model is one of the nonequilibrium growth models. Patterns forming in the diffusive systems are isomorphic to DLA, since the Laplace equation underlies the diffusive systems.[12] The pattern formation in the viscous fingering at an infinite viscosity ratio is a good example.[11] The fractal nature of the aggregate has been analyzed by computational, experimental, and analytical methods. Several analytical attempts, including mean-field theories[13-16] and renormalization-group methods,[17,22] have been made to calculate the fractal dimension and the multifractal structure[23,24] of the growth probability distribution. Several approaches to simple generalizations of the DLA model have been carried out to take into account the finite viscosity ratio,[25,26] sticking probability,[23,27] surface tension,[28-30] particle drift,[31-33] multiparticle effects,[3,34] and lifetime effects.[35] The crossover phenomena between DLA fractal and nonfractal structures were found by computational and experimental methods. By computer simulation, Meakin[27] found the crossover from the dense structure to the DLA fractal by introducing the sticking probability. The scaling form was presented,

$$M(r,P)=r^{2.11}f(Pr^{0.88}) , \tag{1}$$

where M is the mass of the cluster, r the radius of gyration, and P the sticking probability. By computer simulation Sherwood[25] and King[26] found independently the crossover from the DLA fractal to the dense structure by considering the finite viscosity ratio. Very recently, Lee, Coniglio, and Stanley[36] succeeded in analyzing the crossover from the DLA fractal to the dense structure in viscous fingering at the finite viscosity ratio. They extended the position-space renormalization-group method devised by Nagatani[19] and developed the two-parameter renormalization-group method to study the crossover. They showed the global flow diagram in the two-parameter space and calculated the crossover exponent and crossover radius.

Nagatani[37] also succeeded in analyzing the effect of sticking probability on DLA by using the two-parameter position-space renormalization-group method. It was found that when the sticking probability was small the aggregate had to cross over from the dense structure to the DLA fractal. The crossover from the dense structure to the DLA fractal was consistent with the simulated patterns which were thicker near the starting point than near the periphery and above a characteristic radius that showed up in the fractal structure.[38] Consequently, it was shown that the theoretical result and the computer simulation result for the crossover exponent and crossover radius were consistent with each other.

In this paper, we consider a combined effect of sticking probability and finite viscosity ratio upon the pattern formation in Laplacian growth. By introducing a small sticking probability, the crossover from the dense structure to the DLA fractal occurs. In contrast to the sticking probability, the finite viscosity ratio induces the crossover from the DLA fractal to the dense structure. Thus an open question concerns the internal structure and the asymptotic behavior of DLA in which both sticking probability and finite viscosity ratio are introduced. We study the crossover phenomena between the DLA fractal and the nonfractal structures by using a three-parameter

position-space renormalization-group method. We show a global flow diagram in three-parameter space. With a small sticking probability and a finite viscosity ratio, the system crosses over from the dense structure, through the DLA fractal, finally to the dense structure.

The organization of the paper is as follows. In Sec. II we present the dielectric breakdown model on the diamond hierarchial lattice for DLA with both sticking probability and finite viscosity ratio. In Sec. III we apply the three-parameter position-space renormalization-group method to the dielectric breakdown model. In Sec. IV we show the global flow diagram in the three-parameter space. A two-stage crossover phenomenon is found. In Sec. V we present the summary.

II. MODEL

We consider the basic equations for the viscous fingering problem at a finite viscosity ratio by introducing the sticking probability. In order to simplify the problem, we assume that both fluids are Newtonian with zero interfacial tension. The basic equations governing the viscous fingering are given by

$$k_I \nabla^2 p_I = 0 \quad \text{(for injected fluid)}, \qquad k_D \nabla^2 p_D = 0 \quad \text{(for displaced fluid)}, \tag{2}$$

where p, k, and ∇^2 represent the pressure, permeability, and Laplacian, respectively, and the indices I and D indicate the injected fluid and the dispalced fluid. The velocity field is given by

$$v_i = -k \frac{\partial p}{\partial x_i} . \tag{3}$$

The permeability is proportional to the inverse of the viscosity. The viscosity ratio is defined as $\eta_D/\eta_I (= k_I/k_D)$. The two boundary conditions at the interface must be satisfied. The first boundary condition is given by the continuity property of the velocity,

$$v_I = v_D \quad \text{(on the interface)} . \tag{4}$$

Without the sticking probability, the second boundary condition is given by the condition that the pressure field must be continuous across the interface. We extend the second boundary condition to the case with the sticking probability. In the limit of an infinite viscosity ratio, the extended version of DLA introducing the sticking probability P is equivalent to the Laplacian growth model with the third boundary condition $(1-P)\partial p_D/\partial n - P p_D = 0$,[37] where $\partial p/\partial n$ is the derivative normal to the interface. The second boundary condition with the sticking probability is given by

$$(1-P)\frac{\partial p_D}{\partial n} - P(p_D - p_I) = 0 \quad \text{(on the interface)} . \tag{5}$$

The limiting case of $P=1$ represents the ordinary viscous fingering with $p_D = p_I$. The pressure field is continuous across the interface. In the limit of $P \to 0$, it gives the perfectly reflecting boundary and the Eden model is reproduced since the probability visiting the surface becomes uniform over all the surface sites.

We use an electrostatic analogy to transform the viscous finger problem into a specific type of resistor network problem. We describe the viscous fingering in the dielectric breakdown language. The dielectric breakdown model is isomorphic to the viscous fingering, since both systems are governed by the Laplace equation. For simplicity, we consider the problem on the diamond hierarchial lattice. The position-space renormalization-group approach applied to the hierarchial lattice is comparatively accurate to derive the critical behavior of the system. The diamond hierarchial lattice is constructed by an iterative generation of the base set. Each bond is occupied by the resistor of unit conductance. A constant voltage is applied between the bottom and the top on the diamond hierarchial lattice. The dielectric breakdown proceeds from the bottom to the top. Figure 1 shows the illustration of the breakdown model on the diamond lattice. The thick lines indicate breakdown bonds which construct the breakdown pattern. The bonds on the perimeter of the breakdown pattern are represented by the wavy lines. The thin lines indicate unbroken bonds which are resistors of unit conductance. So the resistor network problem is solved under discrete versions of boundary conditions (4) and (5). Across the interface, current is continuous,

$$I_a = I_s \quad \text{(on the interface)} , \tag{6}$$

where I_a is the current flowing through the bond of the breakdown pattern on the perimeter bond, and I_s the current on the perimeter bond. The discrete version of the second boundary condition is given by

$$(1-P)(\Phi_{ns} - \Phi_s) - P(\Phi_s - \Phi_a) = 0 \quad \text{(on the perimeter bond)} , \tag{7}$$

where Φ_s is the potential of a site on the surface of the breakdown pattern, Φ_{ns} the potential of a site that is the nearest neighbor to the breakdown pattern, and Φ_a the potential of a site just below the interface. The potential gap $\Phi_s - \Phi_a$ is interpreted as the voltage drop which

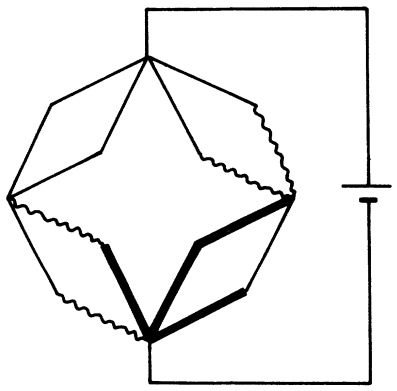

FIG. 1. Illustration of the dielectric breakdown model with the contact resistance. A constant voltage is applied between the bottom and the top. The thick, wavy, and thin lines indicate, respectively, break, growth, and unbroken bonds.

occurs from the contact resistance on the interface. A growth probability proportional to the current is then assigned to the perimeter bond. The breakdown occurs on the perimeter bond according to the growth probability. The interface proceeds to the top just after breaking down. The breakdown process of bonds is assumed to occur one by one. The growth probability p_i at the growing-perimeter bond i is given by

$$p_i \sim I_i \ , \tag{8}$$

where I_i is the local current on the growth bond i. Thus we can describe the viscous fingering at a finite viscosity ratio with the sticking probability in terms of the breakdown model on the resistor network with a contact resistance.

III. RENORMALIZATION-GROUP APPROACH

We develop the position-space renormalization-group method to study both effects of the sticking probability and finite viscosity ratio upon a growth pattern. We consider the renormalization procedure for deriving the three-parameter position-space renormalization-group equations. We derive the renormalization transformations for the sticking probability P, the conductance σ_a of the breakdown bond, and the surface conductance σ_s of the perimeter bond. We will show that the three-parameter renormalization-group equations are given by

$$P' = R_P(P,\sigma_a,\sigma_s) \ , \tag{9}$$

$$\sigma_a' = R_a(P,\sigma_a,\sigma_s) \ , \tag{10}$$

$$\sigma_s' = R_s(P,\sigma_a,\sigma_s) \ . \tag{11}$$

We distinguish between three types of bonds on the lattice before and after a renormalization procedure: (a) breakdown bonds which construct the breakdown pattern, (b) growth bonds which are on the surface of the breakdown pattern and can be successively grown, and (c) unbroken bonds which are in the exterior of the breakdown pattern. The breakdown, growth, and unbroken bonds are, respectively, indicated by the thick, wavy, and thin lines in the figures. We partition all the space of the diamond hierarchial lattice into cells of size $b=2$, (b is the scale factor), each containing a single generator. After a renormalization transformation these cells play the role of "renormalized" bonds. The nth generation of the hierarchial lattice is transformed to the $(n-1)$th generation. The renormalization bonds are then classified into the three types of bonds, similarly to bonds before the renormalization. Figure 2 shows the renormalization procedure. The cell configurations on the upper side are renormalized to the bonds on the bottom side. If the cell is spanned with the bonds occupied by the breakdown bond, then the cell is renormalized as the breakdown bond [Fig. 2(a)]. If the cell is not spanned with the breakdown bond and is the nearest neighbor to the breakdown pattern, then the cell is renormalized, as is the growth bond on the surface [Fig. 2(b)]. When the cell is constructed only by the unbroken bonds and is not the nearest neighbor of the breakdown bond, then the cell is

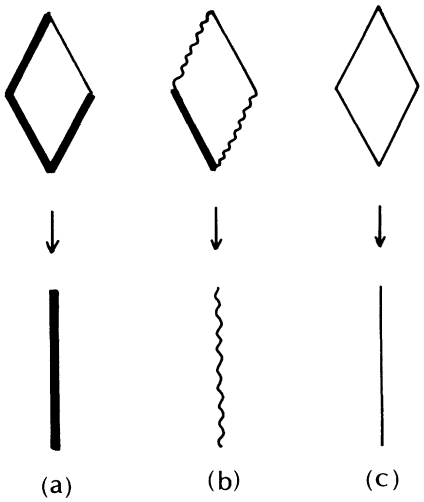

FIG. 2. Renormalization procedure. The cells in the upper side are renormalized to the bonds in the bottom side. There are three types of cells. These cells are, respectively, renormalized as (a) breakdown bond, (b) growth bond, and (c) unbroken bond.

renormalized as the unbroken bond [Fig. 2(c)]. The conductance of the unbroken bond after renormalization remains to be unit value. The conductances of the breakdown bond and the growth bond are transformed to different values from initial values after renormalization. We call the conductance of the growth bond the surface conductance. The sticking probability P is also transformed to a different value P' after renormalization.

We shall first derive the renormalization-group equations for the sticking probability P and the surface conductance σ_s. Figure 3 shows all the configurations of the cell for which it is possible to renormalize as the growth bond. Let us consider the configurational probability C_α with which a particular configuration α appears. The distinct configurations are labeled by α ($\alpha=0,1,2$) in Fig. 3. Configuration (1) is constructed by adding a breakdown bond onto the growth bonds 1 or 2 in configuration (0). The probability with which a breakdown bond adds onto the growth bonds 1 or 2 in configuration (0) is given by the growth probabilities $p_{0,1}$ or $p_{0,2}$ of the growth bonds 1 or 2 in configuration (0). In addition, by adding a breakdown bond to configuration (1), configuration (2) occurs. We here assume that the breakdown proceeds one by one. The configurational probabilities C_α are given by

$$\begin{aligned} C_1 &= C_0(p_{0,1}+p_{0,2}) \ , \\ C_2 &= C_1 p_{1,2} \ , \end{aligned} \tag{12}$$

where $p_{0,1}=p_{0,2}=\frac{1}{2}$. The configurational probability C_0 is determined from the normalization condition

$$\sum_\alpha C_\alpha = C_0 + C_1 + C_2 = 1 \ . \tag{13}$$

Consider the resistor network problem for cells which can be renormalized as the growth bond. The electric

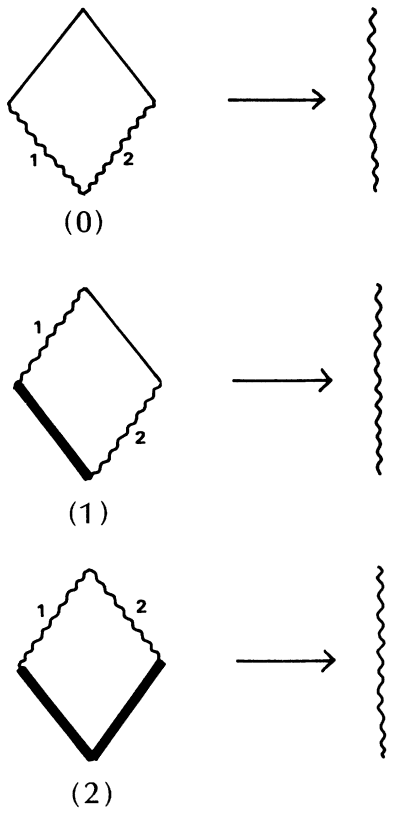

FIG. 3. All distinct configurations of the cell that are possible to renormalize as the growth bond. The circuit on the left-hand side is renormalized to that on the right-hand side in such a way that they are electrically equivalent.

fields within the cell are determined by the sticking probability P, the surface conductance σ_s, and the conductivity σ_a of the breakdown bond. We solve the resistor network problem for deriving the renormalization functions (9) and (11) of the sticking probability P and the surface conductance σ_s. We apply the unit voltage between the top and the bottom for each cell. Figure 3 shows the resistor network problem for configuration (0). The resistor network consisting of the four bonds on the left-hand side is transformed to the single resistor with the equivalent electric property. By using the boundary condition (7), the voltages and the currents within the cell are determined. The total current and the total conductance of the cell are given by

$$I_0=2P\sigma_s/(1+P\sigma_s)\ ,$$
$$\sigma_0'=2\sigma_s/(1+\sigma_s)\ . \tag{14}$$

The voltage V_s' on the surface of the renormalized bond is determined from

$$(1-P_0')(1-V_s')-P_0'V_s'=0\ , \tag{15}$$

where P_0' is the renormalized sticking probability. The total current flowing in the cell is equal to the current flowing through the renormalized bond

$$I_0=\sigma_0'(1-V_s')\ . \tag{16}$$

By using Eqs. (14)–(16), the renormalized sticking probability P_0' is obtained

$$P_0'=(1+\sigma_s)P/(1+P\sigma_s)\ . \tag{17}$$

Similarly to configuration (0), we solve the resistor network problem for the configuration (1) (see Fig. 3). The total current flowing within the cell is given by

$$I_1=\frac{P\sigma_a\sigma_s(1+P\sigma_s)+P\sigma_s(\sigma_a+P\sigma_s)}{(\sigma_a+P\sigma_s)(1+P\sigma_s)}\ . \tag{18}$$

The total conductance of the cell is given by

$$\sigma_1'=\frac{\sigma_s(\sigma_s+2\sigma_a+\sigma_a\sigma_s)}{(1+\sigma_s)(\sigma_a+\sigma_s)}\ . \tag{19}$$

By using the condition that the total current flowing within the cell equals that which is carried through the renormalized bond, the renormalized sticking probability P_1' is given by

$$P_1'=\frac{P(1+\sigma_s)(\sigma_a+\sigma_s)[\sigma_a(1+P\sigma_s)+(\sigma_a+P\sigma_s)]}{(\sigma_s+2\sigma_a+\sigma_a\sigma_s)(\sigma_a+P\sigma_s)(1+P\sigma_s)}\ . \tag{20}$$

The growth probabilities $p_{1,1}$ and $p_{1,2}$ within the cell are given by

$$p_{1,1}=\frac{\sigma_a(1+P\sigma_s)}{2\sigma_a+P\sigma_s+P\sigma_a\sigma_s}\ ,$$
$$p_{1,2}=1-p_{1,1}\ . \tag{21}$$

Similarly, the conductance σ_2' of the cell with configuration (2) is obtained,

$$\sigma_2'=\frac{2\sigma_a\sigma_s}{\sigma_a+\sigma_s}\ . \tag{22}$$

Figure 3 (bottom) shows the resistor network problem for configuration (2). The renormalized sticking probability P_2' of the cell is given by

$$P_2'=\frac{P(\sigma_a+\sigma_s)}{\sigma_a+P\sigma_s}\ . \tag{23}$$

The growth probabilities $p_{2,1}$ and $p_{2,2}$ are given by

$$p_{2,1}=p_{2,2}=\tfrac{1}{2}\ . \tag{24}$$

The renormalized conductance σ_s' of the gorwth bond will be assumed to be given by the most probable value

$$\sigma_s'=\exp\left[\sum_\alpha C_\alpha \ln\sigma_\alpha'\right]\ . \tag{25}$$

Relationship (25), with (14), (19), and (22), presents the renormalization function $\sigma_s'=R_s(P,\sigma_a,\sigma_s)$ for the surface conductance. The renormalized sticking probability P' will be assumed to be given by the mean value

$$P'=\sum_\alpha C_\alpha P_\alpha'\ . \tag{26}$$

Relationship (26), with (17), (20), and (23), presents the renormalization function $P'=R_P(P,\sigma_a,\sigma_s)$ for the stick-

ing probability.

We shall consider here the renormalization for the spanning cluster. The spanning cluster is renormalized as the breakdown bond. Figure 4 shows all the configurations of the spanning cluster. Configurations (1) and (2) of the spanning cluster on the bottom side are constructed from the configurations of the growth cell on the top side. Configuration (1) in Fig. 4 is constructed by adding the breakdown bond onto the growth bond 1 in configuration (1) in Fig. 3. The configurational probability $C_{a,1}$ of configuration (1) is given by

$$C_{a,1}=C_{a,0}P_{1,1}C_1 \ . \tag{27}$$

Configuration (2) in Fig. 4 is constructed by adding the breakdown bond onto the growth bonds 1 or 2 in configuration (2) in Fig. 3. The configurational probability $C_{a,2}$ of configuration (2) is given by

$$C_{a,2}=C_{a,0}(p_{2,1}+p_{2,2})C_2 \ . \tag{28}$$

The unknown constant $C_{a,0}$ is determined by the normalization condition

$$C_{a,1}+C_{a,2}=1 \ . \tag{29}$$

The conductance $\sigma'_{a,1}$ of the cell in Fig. 4(1) is given by

$$\sigma'_{a,1}=(1+\sigma_a)/2 \ . \tag{30}$$

The conductance $\sigma'_{a,2}$ of the cell in Fig. 4(2) is given by

$$\sigma'_{a,2}=\sigma_a/2+\sigma_a/(1+\sigma_a) \ . \tag{31}$$

The renormalized conductance σ'_a of the breakdown bond will be assumed to be given by the most probable value

$$\sigma'_a=\exp(C_{a,1}\ln\sigma'_{a,1}+C_{a,2}\ln\sigma'_{a,2}) \ . \tag{32}$$

Relationship (32), with (30) and (31), presents the renormalization function $\sigma'_a=R_a(P,\sigma_a,\sigma_s)$ for the conductance of the breakdown bond. Equations (25), (26), and (32) give the renormalization equations for three parameters. In the limit of $P=1$, Eqs. (25) and (32) reduce to the result of the viscous fingering at a finite viscosity ratio. In the limit of $\sigma_a\to\infty$, Eqs. (25) and (26) are consistent with the two-parameter renormalization-group equations for DLA with the sticking probability P. Equations (12), (13), (14), (17), and (19)–(32) are simultaneously solved. We find the three nontrivial fixed points $(0,1/\sigma_E^*,0)$, $(1,1/\sigma_{\rm DLA}^*,0)$, and (1,1,1) in the three-parameter space $(P,1/\sigma_s,1/\sigma_a)$ where $\sigma_E^*=2.611$ and $\sigma_{\rm DLA}^*=2.123$. At the fixed point $(0,1/\sigma_E^*,0)$, the growth probabilities $p_{\alpha,i}$ give $\frac{1}{2}$ for all the growth bonds in configurations (0), (1), and (2) in Fig. 3. The growth probability over the whole system becomes uniform over all the surface bonds. The fixed point $(0,1/\sigma_E^*,0)$ corresponds to the Eden model. It is called the first Eden point. The fixed point $(1,1/\sigma_{\rm DLA}^*,0)$ gives the ordinary DLA. It is called the DLA point. The fixed point (1,1,1) gives the result of the viscous fingering at the viscosity ratio 1. The fixed point also corresponds to the Eden model. It is called the second Eden point. In Sec. IV we study the stability of the fixed points in the three-parameter space $(P,1/\sigma_s,1/\sigma_a)$. The global flow in the three-parameter space will be obtained. The crossover phenomena will be investigated.

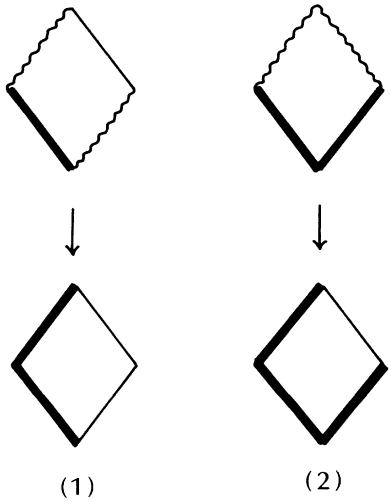

FIG. 4. All distinct configurations of the spanning cluster, which are renormalized as the breakdown bond, are shown on the bottom side. Configurations (1) and (2) are, respectively, constructed from the configurations of the growth bonds shown on the top side.

IV. CROSSOVER BETWEEN THE DLA FRACTAL AND NONFRACTAL

We consider the crossover phenomena between the Eden model and the DLA fractal. First we consider the two limiting cases $\sigma_a\to\infty$ and $P=1$. The case of $P=1$ reproduces the viscous fingering at a finite viscosity ratio. The problem has been analyzed by Lee, Coniglio, and Stanley.[36] The case of $\sigma_a\to\infty$ reproduces the DLA while introducing the sticking probability. Nagatani[37] has presented the renormalizarion-group approach to the problem. We present the results of the two limiting cases for later convenience. Figure 5 indicates the global flow

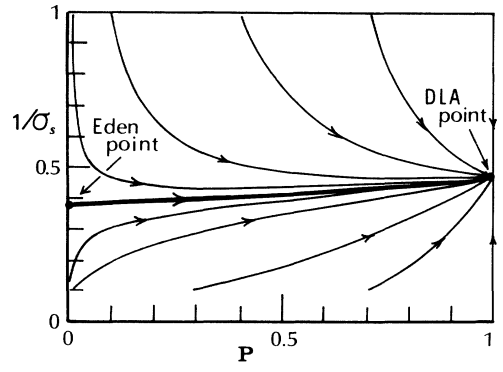

FIG. 5. Global flow diagram in two-parameter space $(P,1/\sigma_s)$ in the limiting case of $\sigma_a\to\infty$. There are two fixed points: the first Eden point and the DLA point. All the renormalization flows are eventually sucked into the DLA point. The crossover line from the Eden to the DLA is indicated by the thick line.

diagram in the two-parameter space $(P,1/\sigma_s)$ in the limiting case of $\sigma_a \to \infty$. The renormalization flows indicated in Fig. 5 are obtained by using (25) and (26) with $\sigma_a \to \infty$. From the renormalization flow, we can determine the stabilities of the two fixed points: the first Eden point and the DLA point. The first Eden point is a saddle point. The DLA point is stable. All the renormalization flows are eventually sucked into the DLA point. It is found from the flow diagrams that there exists a crossover from the dense cluster (the first Eden point) to the DLA fractal (the DLA point). In order to quantify this crossover behavior, we define a crossover exponent ϕ_1 and a crossover radius r_1. The scaling ansatz along the crossover line is proposed:

$$M(r,P)=r^d F_1(Pr^{\phi_1}) , \tag{33}$$

where M is the mass of the cluster, r the radius of gyration, d the embedding dimension, P the sticking probablity, and

$$F_1(x)\sim \begin{cases} 1 & \text{if } x \ll 1 \\ x^{(d_f-d)/\phi_1} & \text{if } x \gg 1 . \end{cases}$$

The d_f is the fractal dimension of DLA. The crossover exponent ϕ_1 is found by linearizing the renormalization equations and calculating the eigenvalues.[37] The crossover radius scales as

$$r_{1\times} \sim P^{-1/\phi_1} , \tag{34}$$

where $\phi_1 = 1.18$.

Figure 6 indicates the global flow diagram in the two-parameter space $(1/\sigma_s,1/\sigma_a)$ in the limiting case of $P=1$. The renormalization flows indicated in Fig. 6 are obtained by using (25) and (32) with $P=1$. From the renormalization flow, we can determine the stabilities of the two fixed points: the second Eden point and the DLA point. The DLA point is a saddle point. The second Eden point is stable. All the renormalization flows are eventually sucked into the second Eden point. It is found from the flow diagram that there exists a crossover from the DLA fractal (the DLA point) to the dense structure (the second Eden point). The crossover from the DLA fractal to the dense structure is in contrast to that found above: the crossover from the dense cluster to the DLA fractal. In order to quantify this crossover behavior, we define a crossover exponent ϕ_2 and a crossover radius $r_{2\times}$. The scaling ansatz along the crossover line is proposed:

$$M(r,(1/\sigma_a))=r^{d_f}F_2((1/\sigma_a)r^{\phi_2}) , \tag{35}$$

where

$$F_2(x)\sim \begin{cases} 1 & \text{if } x \ll 1 \\ x^{(d-d_f)/\phi_2} & \text{if } x \gg 1 . \end{cases}$$

The crossover exponent ϕ_2 is found by linearizing the renormalization equations and the eigenvalues. The crossover radius scales as

$$r_{2\times} \sim (1/\sigma_a)^{-1/\phi_2} , \tag{36}$$

where $\phi_2 = 1.0$.

We study the combined effect of the sticking probablity and the finite viscosity on the cluster structure. To find the global flow diagram in the three-parameter space $(P,1/\sigma_s,1/\sigma_a)$, we choose a representative point in the parameter space, and calculate the renormalized sticking probability, the renormalized surface conductance, and the renormalized conductance of the breakdown bond using (26), (25), and (32) to find a new point $(P',1/\sigma_s',1/\sigma_a')$, We repeat this process to find the next point $(P'',1/\sigma_s'',1/\sigma_a'')$, and continue until we approach a stable fixed point. We use some initial points and plot the renormalization flow in the phase space for representative initial points. Figure 7 shows the renormalization flow, obtained by using (25), (26), and (32). From the renormalization flow, we can determine the stabilities of the three fixed points: the first Eden point, the DLA point, and the second Eden point. The first Eden point and the DLA point are unstable saddle points. The second Eden

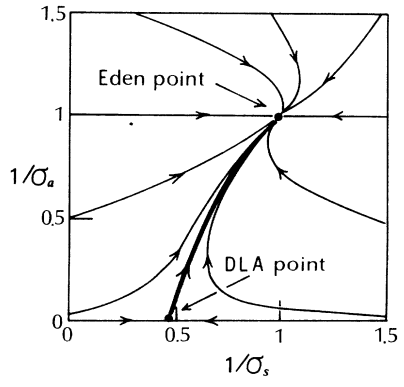

FIG. 6. Global flow diagram in two-parameter space $(1/\sigma_s,1/\sigma_a)$ in the limiting case of $P=1$. There are two fixed points: the DLA point and the second Eden point. All the renormalization flows are eventually sucked into the Eden point.

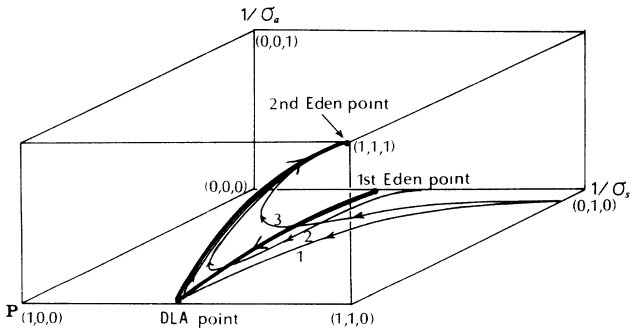

FIG. 7. Global flow diagram in three-parameter space $(P,1/\sigma_s,1/\sigma_a)$. There are three fixed points: the first Eden point, the DLA point, and the second Eden point. A two-stage crossover phenomenon occurs from the dense cluster, through the DLA fractal, finally to the dense structure. The crossover line is indicated by the thick line.

point is stable in every direction. All the renormalization flows are eventually sucked into the second Eden point. The crossover line can be determined by following the renormalization flow which starts from an initial point very close to the first Eden point. It is indicated by the thick line in Fig. 7. Three representative renormalization flows are indicated in Fig. 7. The renormalization flows labeled by 1, 2, and 3 are started from the initial points (0.1, 1, 10^{-5}), (0.001, 1, 10^{-5}), and (0.1, 1, 0.01). It is found from the flow diagram that there exists a two-stage crossover from the dense cluster (the first Eden point), through the DLA fractal (the DLA point), finally to the dense structure (the second Eden point). In order to quantify the double-crossover behavior, we define two crossover exponents ϕ_1 and ϕ_2. We propose the scaling ansatz along the crossover line,

$$M(r,P,(1/\sigma_a))=r^d F_1(Pr^{\phi_1})F_2((1/\sigma_a)r^{\phi_2}) . \quad (37)$$

Here we assume the scaling functions F_1 and F_2 given by (33) and (35). When the sticking probability is small and the finite viscosity ratio is large, the double-crossover phenomena occur from the dense structure, through the DLA fractal, finally to the dense structure. There are already some experimental indications[39] that the qualitative results of our approach may be correct; e.g., the measured finger patterns are thicker near the injection point than near the periphery, and the higher-pressure injection produces the dense pattern.

V. SUMMARY

We propose a Laplacian growth model to study the combined effect of the sticking probability and the finite viscosity ratio upon the cluster structure. We develop a set of position-space renormalization-group equations for DLA with the sticking probability and the finite viscosity ratio. By using the three-parameter position-space renormalization-group method, we find that a two-stage crossover occurs from the dense structure, through the DLA fractal, finally to the dense structure, when the sticking probability is small and the finite viscosity ratio is large.

[1]T. A. Witten and L. M. Sander, Phys. Rev. Lett. **47**, 1400 (1981); Phys. Rev. B **27**, 5686 (1983).

[2]P. Meakin, Phys. Rev. A **27**, 1495 (1983); **27**, 604 (1983); **27**, 2616 (1983).

[3]R. F. Voss, J. Stat. Phys. **36**, 861 (1984).

[4]*Kinetics of Aggregation and Gelation,* edited by F. Family and D. P. Landau (North-Holland, Amsterdam, 1984).

[5]*On Growth and Form,* edited by H. E. Stanley and N. Ostrowsky (Nijhoff, The Hauge, 1985).

[6]*Fractals in Physics,* edited by L. Pietronero and E. Tosatti, (North-Holland, Amsterdam, 1986

[7]P. Meakin, in *Phase Transitions and Critical Phenomena,* edited by C. Domb and J. L. Lebowitz (Academic, New York, 1988), Vol. 12, p. 336.

[8]R. Julien and R. Botet, *Aggregation and Fractal Aggregates* (World-Scientific, Singapore, 1987).

[9]J. Feder, *Fractals* (Plenum, New York, 1988).

[10]*Random Fluctuations and Pattern Growth,* edited by H. E. Stanley and N. Ostrowsky (Kluwer Academic, Dordrecht, 1988).

[11]T. Vicsek, *Fractal Growth Phenomena* (World-Scientific, Singapore, 1989).

[12]L. Pietronero and H. J. Wiesmann, J. Stat. Phys. **36**, 909 (1984).

[13]M. Muthukumar, Phys. Rev. Lett. **50**, 839 (1983).

[14]M. Tokuyama and K. Kawasaki, Phys. Lett. **100A**, 337 (1984).

[15]R. C. Ball, Physica A **140**, 62 (1986).

[16]K. Honda, H. Toyoki, and M. Matsushita, J. Phys. Soc. Jpn. **55**, 707 (1986).

[17]H. Gould, F. Family, and H. E. Stanley, Phys. Rev. Lett. **50**, 686 (1983).

[18]N. Nakanishi and F. Family, Phys. Rev. A **32**, 3606 (1985).

[19]T. Nagatani, J. Phys. A **20**, L381; Phys. Rev. A **36**, 5812 (1987); **38**, 2632 (1988).

[20]L. Pietronero, A. Erzan, and C. Ecertz, Phys. Rev. Lett. **61**, 861 (1988).

[21]J. Lee, P. Alstrom, and H. E. Stanley, Phys. Rev. A **39**, 6545 (1989).

[22]X. R. Wang, Y. Shapir, and M. Rubinstein, Phys. Rev. A **39**, 5974 (1989); J. Phys. A **22**, L507 (1989).

[23]T. C. Halsey, P. Meakin, and I. Procaccia, Phys. Rev. Lett. **56**, 854 (1986).

[24]C. Amitrano, A. Coniglio, and F. di Liberto, Phys. Rev. Lett. **57**, 1016 (1986).

[25]J. D. Sherwood, J. Phys. A **19**, L195 (1986).

[26]P. R. King, J. Phys. A **20**, L529 (1987).

[27]P. Meakin, Ann. Rev. Phys. Chem. **39**, 237 (1988).

[28]T. Vicsek, Phys. Rev. A **32**, 3084 (1985).

[29]L. P. Kadanoff, J. Stat. Phys. **39**, 267 (1985).

[30]R. Tao, M. A. Novotny, and K. Kashi, Phys. Rev. A **38**, 1019 (1988).

[31]P. Meakin, Phys. Rev. B **28**, 5221 (1983).

[32]R. Kapral, S. G. Whittington, and R. C. Desai, J. Phys. A **19**, 1727 (1986).

[33]T. Nagatani, Phys. Rev. A **39**, 438 (1989).

[34]M. Uwaha and Y. Saito, J. Phys. Soc. Jpn. **57**, 3285 (1988).

[35]S. Miyajima, Y. Hasegawa, A. Bunde, and H. E. Stanley, J. Phys. Soc. Jpn. **57**, 3376 (1988).

[36]J. Lee, A. Coniglio, and H. E. Stanley (unpublished).

[37]T. Nagatani, Phys. Rev. A **40**, 7286 (1989).

[38]R. Julien and R. Botet, in *Aggregation and Fractal Aggregates* (Ref. 8), p. 65.

[39]V. Horvath, J. Kertesz, and T. Vicsek, Europhys. Lett. **4**, 1133 (1987).